

# NATIONAL ADVISORY COMMITTEE FOR AERONAUTICS

TECHNICAL NOTE

No. 1426

METHOD OF DESIGNING VANELESS DIFFUSERS AND EXPERIMENTAL  
INVESTIGATION OF CERTAIN UNDETERMINED PARAMETERS

By W. Byron Brown and Guy R. Bradshaw

Flight Propulsion Research Laboratory  
Cleveland, Ohio

**FOR REFERENCE**

NOT TO BE TAKEN FROM THIS ROOM

NACA LIBRARY  
LANGLEY MEMORIAL AERONAUTICAL  
LABORATORY  
Langley Field, Va.



Washington  
September 1947



3 1176 01425 8918

NATIONAL ADVISORY COMMITTEE FOR AERONAUTICS

TECHNICAL NOTE NO. 1426

METHOD OF DESIGNING VANELESS DIFFUSERS AND EXPERIMENTAL  
INVESTIGATION OF CERTAIN UNDETERMINED PARAMETERS

By W. Byron Brown and Guy R. Bradshaw

SUMMARY

A method of designing vaneless diffusers, using data given for simple conical diffusers, is presented. The rate of expansion of the flow area through the diffuser is found in terms of an equivalent cone laid off along the logarithmic spiral having an angle equal to that for the optimum flow condition of the impeller.

A family of diffusers with equivalent cone angles of  $4^\circ$ ,  $6^\circ$ , and  $8^\circ$ , all having the same throat height, was designed and experimentally studied. A second series of diffusers, having throats equal to 62, 72, and 93 percent of the height just beyond the impeller outlet, and all having the cone angle corresponding to the best performance in the first tests ( $6^\circ$ ), was then constructed. A diffuser with the  $6^\circ$  equivalent cone angle and a contraction ratio of 0.72 was found to have the highest efficiency, about 0.83 at the diffuser exit at tip speeds of 900 to 1200 feet per second. The improved performance with the forementioned design parameters was particularly noticeable at high loads and tip speeds.

INTRODUCTION

The demand for improved diffuser performance becomes increasingly insistent with refinement in impeller design and emphasis on high compressor efficiencies. As a device for achieving high efficiency in the centrifugal-type compressor over a wide range of air flows and tip speeds, the vaneless-type diffuser has certain inherent advantages over the vanned-type diffuser. At the impeller outlet the distribution of velocities, both in magnitude and direction, precludes the possibility of introducing fixed vanes that will provide the optimum angle of attack for all the incident air at any one operating condition, and changes in this angle with volume flow and tip speed still further reduce the probability of satisfactory incidence. Moreover, the presence of diffuser vanes near the impeller outlet may result in relative velocities equal to that of sound, with consequent shock losses. On the other hand, continuous diffusion of

supersonic circumferential-velocity components apparently can be accomplished in the vaneless diffuser and changes in the flow angle, in the absence of vanes, apparently will produce no serious increases in diffuser losses.

The design of vaneless diffusers involves two closely related problems. In order that the diffusion may be efficiently accomplished, the nonuniform flow at the impeller outlet should be converted into a steady flow with a uniform velocity profile before a serious attempt is made to reduce the axial and radial components of velocity. This transformation is a function of the transition section, the passage from the impeller outlet to the narrowest part (throat) of the diffuser passage. The function of the diffuser proper is to convert the dynamic energy of the advancing flow into pressure as rapidly as possible without incurring flow separation at the most adverse operating condition. Because diffusion of the tangential component is essentially a function of radial distance only, any acceleration of the diffusion process must be effected by increasing the rate of diffusion of the radial and axial components of velocity, that is, by increasing the rate of expansion of the flow area.

An efficient diffuser should perform both of these operations with the smallest possible losses and at the same time, because of the penalty on size, in the smallest possible frontal area. Inasmuch as detailed information concerning flow conditions in the transition section is lacking, only rather general design criteria can be set up; for example, gradual changes in direction of the walls and gradual changes in flow area, particularly from small to large areas. In the absence of satisfactory theoretical criteria for the determination of the optimum rate of diffusion in a vaneless diffuser, the optimum rate of area expansion, as a first approximation, can be made the same for the vaneless diffuser as the optimum rate for a simple conical diffuser. Experiments with such diffusers (reference 1) have shown that maximum efficiency is associated with divergence angles of  $5^\circ$  to  $8^\circ$ .

The analytical problem is therefore: (a) to determine a transition profile that, conforming to the preceding criteria, blends smoothly with both impeller outlet and diffuser entrance, and (b) to fix such values for the distance between the two plates of the diffuser proper that the rate of area expansion along a prescribed flow path shall be the same as the rate of area expansion of an equivalent cone having the optimum divergence angle. When equations incorporating the conditions on transition and diffuser sections are set up, a variable parameter may remain undetermined in each case. The optimum value of the appropriate parameter for each section may then be experimentally determined.

The method used in the design of the diffusers and the results, in terms of compressor performance, of varying the parameters associated with the transition section and the diffuser proper are presented. Five 34-inch-diameter vaneless diffusers were studied. Three diffusers were designed with the same transition-section parameter but equivalent cone angles of  $4^\circ$ ,  $6^\circ$ , and  $8^\circ$ . The transition section of the diffuser showing the best performance was then so modified as to give first a wider, then a narrower, throat than the original, and the effect of these modifications was experimentally investigated.

### SYMBOLS

The following symbols are used:

$C$	constant of integration
$c_p$	specific heat at constant pressure, foot-pounds per pound $^\circ F$
$D$	hydraulic diameter, inches
$f$	friction coefficient (ratio of shear stress to dynamic pressure)
$g$	acceleration of gravity, 32.14 feet per second per second
$h$	passage height perpendicular to rear shroud, inches
$K$	constant dependent on $\alpha_\theta$
$l$	distance measured along flow path, inches
$M$	angular momentum per unit mass ( $rU_\theta$ ), feet per second $\times$ inches
$P$	total pressure, inches of mercury absolute
$P_2/P_1$	compressor pressure ratio, ratio of outlet total pressure to inlet total pressure
$p$	static pressure, inches of mercury absolute
$Q_{t,1}/\sqrt{\theta}$	corrected volume flow, cubic feet per minute

$Q_{t,1}/\sqrt{\theta} D_2^2$	specific capacity, cubic feet per minute per square foot (where $D_2$ is impeller-outlet diameter)
$R$	gas constant, 53.4
$r$	radial distance from axis, inches
$r_c$	radius of equivalent cone section, inches
$r_t$	radius of curvature for transition-section front shroud, inches
$T$	total temperature, $^{\circ}R$
$t$	static temperature, $^{\circ}R$
$U$	absolute air velocity, feet per second
$U_a$	component of air velocity in axial direction, feet per second (fig. 1)
$U_m$	meridional component of air velocity (normal to $U_t$ and parallel to rear shroud of diffuser), feet per second (fig. 1)
$U_r$	component of air velocity in radial direction, feet per second (fig. 1)
$U_{\theta}$	component of air velocity tangential to circle of radius $r$ , feet per second (fig. 1)
$V$	impeller tip speed, feet per second
$W$	mass air flow, pounds per second
$\alpha$	flow angle (angle between $U$ and $U_{\theta}$ ), degrees (fig. 1)
$\beta$	angle between diffuser rear shroud and radial direction, degrees (fig. 1)
$\gamma$	ratio of specific heats
$\delta$	half-angle of equivalent cone along design path, degrees
$\epsilon$	angle between front and rear shrouds at impeller outlet, degrees

$\eta_{ad}$	adiabatic efficiency
$\theta$	ratio of actual inlet stagnation temperature to NACA standard sea-level temperature
$\lambda$	contraction ratio for transition section ( $h_e/h_o$ )
$\rho$	air density, pounds per cubic foot
$\varphi$	angle between front and rear shrouds at diffuser entrance (after transition section), degrees

## Subscripts:

e	entrance to diffuser section (transition-section exit)
o	impeller outlet (transition-section entrance)

## DESIGN THEORY

The two phases of diffuser operation, transformation of the chaotic flow at the impeller outlet into a uniform stream and conversion of the kinetic energy of the radial and axial components of velocity into pressure, may conveniently be separately considered, although neither component of the diffuser can be designed independently of the other. The diffuser proper will be considered first; then the requirements for a smooth transition section from impeller to diffuser will be established.

Diffuser section. - With respect to the diffuser proper, the problem as defined is the determination of a diffuser profile that will provide a rate of increase of area along a predetermined flow path the same as that of a conical diffuser of divergence angle  $2\delta$ . Because of compressibility, designing for only one operating condition is possible. At this design condition, the air leaves the transition section at some angle  $\alpha_e$  that is assumed to remain constant throughout the diffuser. The design path is therefore a logarithmic spiral, or more precisely, because of an axial component of flow in this instance, a helix on a cylinder whose directrix curve is a logarithmic spiral (fig. 2). A straight line equal in length to the arc length of the helix forms the axis of the equivalent cone.

At any distance  $l$  along the design path

$$2\pi r h \sin \alpha_e = \pi r_o^2 \quad (1)$$

where  $2\pi rh \sin \alpha_e$  is the area of the diffuser passage normal to the flow direction and  $\pi r_c^2$  is the area of the corresponding section of the equivalent cone. The quantities  $r$ ,  $h$ , and  $r_c$  are all functions of  $l$ .

When equation (1) is differentiated with respect to  $l$ ,

$$\sin \alpha_e \frac{d(rh)}{dl} = r_c \frac{dr_c}{dl} \quad (2)$$

But

$$dr_c/dl = \tan \delta$$

and

$$\frac{d(rh)}{dl} = \frac{d(rh)}{dr} \frac{dr}{dl} = \frac{d(rh)}{dr} \sin \alpha_e \cos \beta$$

If these substitutions are made in equation (2), the value of  $r_c$  is introduced from equation (1), and the equation is rearranged,

$$\frac{\frac{d}{dr}(rh)}{\sqrt{rh}} = \frac{\sqrt{2} \tan \delta}{\sin^{3/2} \alpha_e \cos \beta} = K \quad (3)$$

where  $K$  is adjustable through its dependence on  $\alpha_e$ .

If equation (3) is rewritten in the form

$$K dr = \frac{d(rh)}{\sqrt{rh}}$$

and integrated,

$$Kr = 2 \sqrt{rh} - C \quad (3a)$$

where  $C$ , a constant of integration, depends upon the profile and the height of the transition section, which fix  $h_e$ ,  $r_e$ , and  $\alpha_e$ . It is determined by the conditions that the diffuser entrance shall have the same height as the transition-section exit, and that the two sections, at their junction, shall have common tangents at both front and rear shrouds.

When equation (3a) is solved for  $h$

$$h = \frac{K^2 r}{4} + \frac{KC}{2} + \frac{C^2}{4r} \quad (4)$$

Equation (4) gives, in terms of constants that must be adjusted to the transition section, the value that  $h$  must have at all radii in order that the rate of area expansion along the design path shall be the same as that of a cone of half-angle  $\delta$ .

Transition section. - Primarily because of the extreme complexity of the flow conditions at the impeller outlet, it is difficult to impose on the transition section any more definite requirement than that it shall have gradual changes in both the direction of the walls and the flow area. For simplicity this study is limited to a section whose front wall is a circular arc, whereas the rear wall, after turning gradually through an angle of  $5^\circ$  in a radial direction, continues as a straight line. The  $5^\circ$  bend was necessitated by the dimensions of the experimental setup. The requirement for smooth transition from impeller to diffuser implies five geometrical conditions:

(1) The relation between passage heights at entrance and exit of the transition section may be expressed

$$h_e = \lambda h_o \quad (5)$$

where  $\lambda$  is here regarded as an arbitrary constant whose optimum value is to be determined experimentally.

(2) The fundamental equation for the determination of  $h$  (equation (4)) becomes, at the exit from the transition section

$$h_e = \frac{K^2 r_e}{4} + \frac{KC}{2} + \frac{C^2}{4r_e} \quad (4a)$$

(3, 4) From the geometry of the configuration shown in figure 3,

$$r_e - r_o = r_t (\sin \epsilon + \sin \varphi) \cos \beta \quad (6)$$

and

$$h_e + r_t \cos \varphi = h_o + r_t \cos \epsilon \quad (7)$$

(5) The requirement that the diffuser and transition sections have the same slope at the diffuser entrance yields

$$\frac{\tan \varphi}{\cos \beta} = \frac{dh}{dr} = \frac{K^2}{4} - \frac{C^2}{4r_e^2} \quad (8)$$

The four physical conditions to be met are the continuity equation

$$W = \rho \frac{2\pi r h U_m}{144} \quad (9)$$

the adiabatic relation (appendix A),

$$\rho = \frac{P}{RT} \left( 1 - \frac{U^2}{2gc_p T} \right)^{2.53} \quad (10)$$

the equation for the loss of total pressure (appendix B),

$$dP = - \frac{f}{g} \frac{\csc \alpha \sec^2 \alpha}{hRT} \frac{M^2 dr P}{r^2 \left( 1 - \frac{U^2}{2gc_p T} \right) \cos \beta} \quad (11)$$

and the angular-momentum equation (reference 2), which in the present notation becomes

$$\frac{dM}{M} = - f \frac{\csc \alpha_e}{h_e} \frac{dr}{\cos \beta} \quad (12)$$

where the magnitude of  $f$  is one-fourth the magnitude of the friction factor of reference 2. The factor  $\cos \beta$  appears here in the denominator because the element of design path of reference 2 is in a plane normal to the axis.

#### DESIGN PROCEDURE

The geometry of the impeller outlet, as well as the mean flow conditions and the state of the air at that location, is assumed to be known; that is, the quantities  $r_e$ ,  $h_e$ ,  $W$ ,  $T_o = T_2$ ,  $P_o$ ,  $U_{\theta, o}$ , and  $V$  are given. From these quantities, the meridional component of the air velocity  $U_{m, o}$  and the angle  $\alpha_o$ , where

$$\tan \alpha_o = \frac{U_{r, o}}{U_{m, o}}$$

can be found as also can the density  $\rho_0$ . The successive steps in the design are then as follows:

1. The value of  $h_e$  was determined from the relation  $h_e = \lambda h_0$ . The initial value of  $\lambda$  was necessarily arbitrary. For the conditions of this investigation, the optimum value of  $\lambda$  subsequently was experimentally found to be approximately 0.7.

2. Inasmuch as a direct solution for the unknown variables leads to excessively complicated equations, a trial-and-error approach is more practicable. The angle  $\varphi$  is necessarily small because of the small values of  $\delta$ . As a first approximation to the solution,  $\varphi$  may therefore be assumed equal to 0. Equations (6) and (7) then take the form

$$r_e - r_0 = G \sin \epsilon \cos \beta$$

where

$$G = \frac{h_0 - h_e}{1 - \cos \epsilon}$$

From the preceding equations

$$r_e - r_0 = \frac{h_0 - h_e}{1 - \cos \epsilon} \sin \epsilon \cos \beta$$

This value of  $r_e - r_0$  was retained and is later used to find the corrected value of  $\varphi$ .

3. Equation (12) was integrated from entrance to exit of the transition section to determine the angular momentum of the flow at the transition exit. This integration provides the relation

$$\log M_e = -f \frac{\csc \alpha}{h} (r_e - r_0) + \log M_0 \quad (13)$$

From continuity considerations and the geometry of the flow

$$\frac{\csc \alpha}{h} = \frac{2\pi}{W} \rho r U$$

The magnitude of  $rU_\theta$ , and of  $rU$ , decreases slowly through the transition section whereas that of  $\rho$  increases slightly. The magnitude of  $(\csc \alpha)/h$  was therefore assumed to be constant through the section and the initial value was used.

4. The circumferential-velocity component at the exit of the transition section was found from the equation

$$U_{\theta,e} = \frac{M_e}{r_e}$$

5. When the value of  $M$  from equation (13),

$$M = M_0 e^{-f \frac{\csc \alpha}{h} (r - r_0)} \quad (14)$$

is substituted in equation (11) and the equation integrated between the limits  $P_0$  and  $P_e$ , the value for  $P_e$  is given in the form

$$\log P_e = - \frac{f}{g} \frac{\csc \alpha}{h} \frac{\sec^2 \alpha}{RT \cos \beta} \int_{r_0}^{r_e} \frac{e^{-f \frac{\csc \alpha}{h} (r - r_0)}}{r^2 \left(1 - \frac{U^2}{2gc_p T}\right)} dr + \log P_0 \quad (15)$$

In equation (15) and the following equation, an approximate value of  $U$  is needed. A sufficiently accurate value can be obtained from the equation  $U^2 = U_m^2 + U_{\theta}^2$  by using the value of  $U_m$  at the transition-section entrance.

6. The density  $\rho_e$  at the exit of the transition section was found from the relation

$$\rho_e = \frac{1.322 P_e}{T} \left(1 - \frac{U^2}{2gc_p T}\right)$$

7. Values of  $\varphi$  and  $\alpha$  can then be calculated from the following equations, which are developed in appendix C:

$$\tan \varphi = B + G \cot \alpha_e \quad (16)$$

where

$$B = 2 \tan \frac{1}{2} \epsilon - \frac{2h_e \cos \beta}{r_e - r_0}$$

$$G = \frac{144 W \cos \beta}{\pi \rho_e M_e (r_e - r_0)}$$

and

$$\frac{144 W \cot \alpha_e}{2\pi M \rho r_e} = \frac{\tan^2 \delta}{\sin^3 \alpha_e \cos^2 \beta} - \frac{\tan \varphi}{\cos \beta} + \frac{\tan \delta}{\sqrt{2} \sin^3 \alpha_e \cos \beta} \sqrt{\frac{2 \tan^2 \delta}{\sin^3 \alpha_e \cos^2 \beta} - \frac{4 \tan \varphi}{\cos \beta}} \quad (17)$$

A trial-and-error method was employed in the solution of these equations. A value for  $\varphi$  was assumed and equation (16) was solved for  $\alpha_e$ . These values were then inserted in equation (17) and, by inspection, a second approximation to  $\varphi$  was chosen, such as to reduce the existing inequality, and the procedure was repeated. Three or four trials were usually sufficient to give an identity for equation (17).

8. The constants  $K$  and  $C$ , which determine the profile of the passage, were then obtained from equations (3) and (8), respectively:

$$K = \frac{\sqrt{2} \tan \delta}{\sin^{3/2} \alpha_e \cos \beta}$$

and

$$C = r_e \sqrt{K^2 - \frac{4 \tan \varphi}{\cos \beta}}$$

The value of  $r_t$  was found from equation (6)

$$r_t = \frac{r_e - r_o}{(\sin \epsilon + \sin \varphi) \cos \beta}$$

9. As a check, the channel height was then calculated from the two equations

$$h_e = h_o + r_t (\cos \epsilon - \cos \varphi)$$

$$h_e = \frac{K^2 r_e}{4} + \frac{KC}{2} + \frac{C^2}{4r_e} \quad (4a)$$

## DESIGNS TESTED

The design theory leaves undetermined the optimum values of both the contraction ratio  $\lambda$  and the equivalent cone angle  $\delta$ . It was therefore desirable that the experimental program investigate the effect of varying each of these parameters. Three vaneless diffusers of 34-inch diameter were built and tested. For each of these diffusers, the value of  $\lambda$  was 0.72 and that of  $\alpha$  was  $26^\circ$ , corresponding to the best impeller performance. The equivalent cone angles of the three diffusers were  $4^\circ$ ,  $6^\circ$ , and  $8^\circ$  (fig. 4). The diffuser that gave the best performance in these tests ( $6^\circ$  equivalent cone) was then so modified as to have values of  $\lambda$ , first, of 0.93 and then of 0.62 (fig. 5).

The same rear diffuser wall was used in all the diffusers. The magnitude of the angle  $\beta$  ( $25^\circ$ ) was dictated by the dimensions of the test rig, the corresponding outlet angle of the impeller being about  $30^\circ$ . Even then, this  $25^\circ$  angle was slightly large and the rear shroud had to be curved forward for the last 4 inches. The effect of this curvature near the diffuser exit appeared to be negligible.

In the diffuser for which  $\lambda = 0.93$ , the transition section was very short; the  $6^\circ$  diffuser section started about 0.7 inch, radially, beyond the impeller outlet. (See fig. 5.) The transition section having  $\lambda = 0.62$  necessitated abandoning the design condition that the impeller front shroud and the wall of the transition section have a common tangent at the transition entrance. The entrance passage was so proportioned that the resultant air velocity was constant for about the first  $3/4$  inch in the transition section, which resulted in a relatively abrupt change in wall direction (fig. 5).

Tables I to III show details of the profiles of the different diffusers.

## APPARATUS AND TESTS

A variable-component test rig (reference 3) was employed in this investigation. The mixed-flow impeller used is shown in figure 6 and a sketch of the impeller and the diffuser, in figure 7. Standard instrumentation was used where applicable. In addition, total-pressure tubes, which provided data for direct calculation of the efficiency of the impeller-diffuser combination, were installed at the diffuser exit (except in the  $4^\circ$  diffuser). A single tangential collector outlet was used instead of two radial collector outlets, but previous investigations showed no appreciable difference in the instrument readings for the two configurations.

Each diffuser was investigated at actual tip speeds of 900, 1100, 1200, and 1300 feet per second (except the 4° diffuser, which was not run at 1300 ft/sec), and the data were subsequently corrected to standard atmospheric conditions. For each tip speed, the flow range was from open throttle to surge.

## RESULTS AND DISCUSSION

In the comparison of the performance of diffusers with different values of contraction ratio  $\lambda$  and equivalent cone angle  $\delta$ , efficiency at the diffuser exit rather than over-all efficiency was chosen as the most direct, practicable measure of the diffuser efficiency. Although this procedure involves the tacit assumption that no change occurs in impeller performance with the changes in diffuser variables, measurements of total pressure at the impeller outlet, which would allow the isolation of diffuser performance, are, in general, rather unreliable.

Efficiencies at the diffuser exit for the three diffusers having  $\lambda = 0.72$  and equivalent cone angles of 4°, 6°, and 8°, are shown in Figure 8. The adiabatic efficiency was found by the procedure recommended for determining over-all efficiency (reference 4) except that the arithmetic mean of the total pressures at four stations across the diffuser exit was substituted for the corresponding quantity at the outlet measuring station. For the present purpose, efficiency is plotted against load coefficient, inasmuch as this parameter, being related to the flow angle  $\alpha_e$ , facilitates comparison of efficiencies at approximately equivalent operating conditions.

Inasmuch as total-pressure tubes were not installed at the diffuser exit of the 4° diffuser, the impeller-diffuser efficiencies were computed from a collector correlation that gave the static pressure at the diffuser exit and the calculated exit velocities.

The curves of figure 8 indicate relatively high performance of the 6° diffuser at high loads. The peak efficiency of the 6° diffuser at high tip speeds is 4 to 5 points above that for either of the other two diffusers. In general, the 4° diffuser has a definite advantage at low loads. For the 4° diffuser, a decrease in load coefficient (and so of  $\alpha_e$ ) below the value for maximum efficiency seems to be associated with smaller losses in efficiency than for the 6° or 8° diffuser. At values of load coefficient less than the design value, the departure from optimum flow conditions in the 4° is less than in the 6° diffuser, as the tendency to increase  $\alpha$  towards its design value is greater for the smaller

equivalent cone angle. The peak adiabatic efficiencies at the diffuser exit for the three equivalent cone angles and the medium throat are given in the following table:

Diffuser	Peak adiabatic efficiency			
	Actual tip speed (ft/sec)			
	900	1100	1200	1300
4°	0.83	0.82	0.78	-----
6°	.84	.84	.83	0.79
8°	.85	.80	.77	.75

For the impeller investigated, an equivalent cone angle of approximately 6° gives the highest peak efficiency at high tip speeds and the highest efficiency at the high values of load coefficient.

Diffuser-exit efficiencies for the 6° diffuser with the three values for  $\lambda$  (0.62, 0.72, 0.93) are shown in figure 9. The medium throat ( $\lambda = 0.72$ ) shows appreciably higher efficiencies at medium and high loads at all tip speeds than either of the others. In this connection it may be recalled that the narrow throat made it impossible to retain at the front shroud the common tangent to the impeller outlet and transition entrance, and deterioration of the flow at high load coefficient might be anticipated. At low load coefficient, the narrow throat quite consistently shows higher efficiencies than the medium or wide throats at the same value of load coefficient.

The following table shows the peak efficiencies at the diffuser exit for the three values of  $\lambda$  used in this investigation with the diffuser having a 6° equivalent cone expansion angle:

$\lambda$	Peak adiabatic efficiency			
	Actual tip speed (ft/sec)			
	900	1100	1200	1300
0.62	0.81	0.78	0.77	0.71
.72	.84	.84	.83	.79
.93	.81	.81	.78	.75

Judged on the basis of peak efficiency and efficiency at medium and high load coefficient; the transition section having a value of  $\lambda$  of 0.72 gives the best results of the three in the present setup.

The over-all performance of the compressor using the  $6^\circ$  diffuser with  $\lambda = 0.72$  is shown in figure 10. Pressure ratios are plotted against corrected volume flow in accordance with recommended procedure (reference 5) with adiabatic efficiencies shown as contour lines. Figure 11 compares the over-all performance of the compressor when the  $6^\circ$ , medium-throat ( $\lambda = 0.72$ ), vaneless diffuser was used with the performance of the same impeller with the manufacturer's vaned diffuser, at actual tip speeds of 800 and 1100 feet per second. Pressures at the standard measuring station in the outlet pipe were used in computing these efficiencies. Data for the vaned diffuser were obtained on the same rig and by the same techniques as those for the investigation of the vaneless diffusers. The wider operating range of the vaneless diffuser at reasonable efficiencies is apparent at both tip speeds, and peak efficiencies are higher with the vaneless diffuser by about 6 points and occur at somewhat higher load coefficients.

A more extensive investigation using different types of impeller would be required to determine whether these results are generally valid. In particular, the observed variations in performance with the true flow angle  $\alpha$  indicate that the optimum cone angle in the transition section would probably be different for an impeller having a different flow angle at the design point.

#### SUMMARY OF RESULTS

A diffuser-design method was investigated with five vaneless diffusers in combination with a mixed-flow impeller in a variable-component test rig. The five impellers incorporated three different throat heights and three different rates of area expansion (equivalent cone angles). The design method, which left throat height and rate of area expansion as parameters to be experimentally determined, resulted in compressor efficiencies equal to or better than those shown by the vaned diffuser designed for this impeller and retained the characteristically wide operating range of the vaneless diffuser. The diffuser with the  $6^\circ$  equivalent cone angle and a throat-inlet ratio of 0.72 was found to have the highest efficiency, about 0.83 at the diffuser exit at actual tip speeds of 900 to 1200 feet per second. Throughout most of the useful operating range

the  $6^\circ$  equivalent cone angle gave peak efficiencies from 4 to 5 points higher than either the  $4^\circ$  or  $8^\circ$  equivalent cone angle. The medium throat gave higher efficiencies by 3 to 8 points than either of the others at the high tip speeds and load coefficients..

Flight Propulsion Research Laboratory,  
National Advisory Committee for Aeronautics,  
Cleveland, Ohio, June 27, 1947.

## APPENDIX A

## DERIVATION OF EQUATION FOR AIR DENSITY

From the gas law,

$$\rho = \frac{p}{Rt} \quad (18)$$

the relation between total and static pressure,

$$\frac{p}{P} = \left(1 - \frac{U^2}{2gc_p T}\right)^{3.53} \quad (19)$$

and the relation between total and static temperature,

$$\frac{t}{T} = \left(1 - \frac{U^2}{2gc_p T}\right) \quad (20)$$

an expression for density can be obtained in terms of total pressure, temperature, and velocity. Substitution in equation (18) of the value of  $p$  from equation (19) and that of  $t$  from equation (20) yields

$$\rho = \frac{P}{RT} \left(1 - \frac{U^2}{2gc_p T}\right)^{2.53}$$

## APPENDIX B

## DERIVATION OF EQUATION FOR TOTAL-PRESSURE LOSS

The pressure loss required to overcome frictional resistance can be found from an extended form of Bernoulli's equation containing a friction term in addition to the customary terms for pressure and kinetic energy.

The equation, developed in reference 6 in slightly different notation, is

$$\frac{dp}{\rho} + \frac{UdU}{g} + \frac{4fU^2dl}{2gD} = 0$$

From the general gas law  $\rho = p/Rt$ , and substitution of this value for  $\rho$  yields

$$Rt \frac{dp}{p} + \frac{UdU}{g} = - \frac{4fU^2dl}{2gD}$$

The relation between total and static pressures

$$\frac{p}{P} = \left(1 - \frac{U^2}{2gc_pT}\right)^{\frac{\gamma}{\gamma-1}}$$

when differentiated logarithmically yields

$$\frac{dp}{p} - \frac{dP}{P} = - \frac{\gamma}{\gamma-1} \left( \frac{\frac{2UdU}{2gc_pT}}{1 - \frac{U^2}{2gc_pT}} \right)$$

If this equation is multiplied through by  $Rt$ , if the value  $c_p/R$  is substituted for  $\gamma/(\gamma-1)$ , and if the relation between total and static temperatures,

$$\frac{t}{T} = 1 - \frac{U^2}{2gc_pT}$$

is introduced, the equation becomes

$$Rt \frac{dp}{p} + \frac{UdU}{g} = Rt \frac{dP}{P}$$

Bernoulli's equation can thus be written in terms of total pressure

$$Rt \frac{dP}{P} = - \frac{4fU^2 dl}{2gD}$$

For the vaneless diffuser

$$dl = dr \csc \alpha / \cos \beta$$

$$U^2 = \frac{M^2}{r^2} \sec^2 \alpha$$

$$t = T \left( 1 - \frac{U^2}{2gc_p T} \right)$$

and

$$D = 2h$$

Substitution of these values gives

$$\frac{dP}{P} = - \frac{f}{g} \frac{\csc \alpha \sec^2 \alpha}{hRT} \frac{M^2 dr}{r^2 \left( 1 - \frac{U^2}{2gc_p T} \right) \cos \beta}$$

## APPENDIX C

DERIVATION OF EQUATIONS FOR  $\varphi$  AND  $\alpha_e$ 

The two equations in  $\varphi$  and  $\alpha_e$  can be found as follows:

$$r_e - r_o = r_t (\sin \epsilon + \sin \varphi) \cos \beta \quad (6)$$

$$h_o - h_e = r_t (\cos \varphi - \cos \epsilon) \quad (7a)$$

Elimination of  $r_t$  results in

$$\frac{r_e - r_o}{h_e - h_o} = \frac{(\sin \epsilon + \sin \varphi) \cos \beta}{\cos \varphi - \cos \epsilon}$$

Solving for  $h_o - h_e$  yields

$$\begin{aligned} h_o - h_e &= \frac{r_e - r_o}{\cos \beta} \frac{\cos \varphi - \cos \epsilon}{\sin \varphi + \sin \epsilon} \\ &= \frac{r_e - r_o}{\cos \beta} \left[ \frac{-2 \sin \frac{1}{2}(\varphi + \epsilon) \sin \frac{1}{2}(\varphi - \epsilon)}{2 \sin \frac{1}{2}(\varphi + \epsilon) \cos \frac{1}{2}(\varphi - \epsilon)} \right] \\ &= \frac{r_e - r_o}{\cos \beta} \tan \frac{\varphi - \epsilon}{2} = \frac{r_e - r_o}{\cos \beta} \frac{\tan \frac{1}{2} \epsilon - \tan \frac{1}{2} \varphi}{1 + \tan \frac{1}{2} \epsilon \tan \frac{1}{2} \varphi} \end{aligned}$$

For convenience, let

$$A = 1 + \tan \frac{1}{2} \epsilon \tan \frac{1}{2} \varphi$$

then

$$\tan \frac{1}{2} \varphi = \tan \frac{1}{2} \epsilon - \frac{(h_o - h_e) A \cos \beta}{r_e - r_o}$$

Because  $\varphi$  is a small angle,

$$\tan \frac{1}{2} \varphi = \frac{1}{2} \tan \varphi$$

and

$$\tan \varphi = 2 \tan \frac{1}{2} \epsilon - \frac{2h_o A \cos \beta}{r_e - r_o} + \frac{2h_e A \cos \beta}{r_e - r_o}$$

From equation (9)

$$h_e = \frac{144W}{2\pi r_e \rho_e U_{m,e}} = \frac{144W}{2\pi \rho (r_e U_{\theta,e})} \cot \alpha_e$$

and

$$r_e U_{\theta,e} = M_e$$

Substitution of these quantities in the equation for  $\tan \varphi$  results in

$$\tan \varphi = 2 \tan \frac{1}{2} \epsilon - \frac{2h_o A \cos \beta}{r_e - r_o} + \frac{144W A \cos \beta}{\pi M_e \rho_e (r_e - r_o)} \cot \alpha_e$$

In all actual cases,  $A$  will be very nearly equal to unity. For example, if  $\epsilon = 20^\circ$  and  $\varphi = 1^\circ$  then  $\frac{1}{2} \tan \frac{1}{2} \epsilon \tan \varphi$  is 0.0015 so that  $A$  differs from 1 by only 0.15 percent. After using  $A = 1$  as a first approximation, a more precise value can be found, if desired, after  $\varphi$  is known but this refinement is in general unnecessary.

If  $A$  is taken equal to 1, the equation for  $\tan \varphi$  can be written

$$\tan \varphi = B + G \cot \alpha_e \quad (16)$$

where

$$B = 2 \tan \frac{1}{2} \epsilon - \frac{2h_o \cos \beta}{r_e - r_o}$$

$$G = \frac{144W \cos \beta}{\pi \rho_e M_e (r_e - r_o)}$$

The quantities  $B$  and  $G$  can be found and give one of the two equations in  $\varphi$  and  $\alpha_e$ .

The second equation involving  $\varphi$  and  $\alpha_e$  is obtained from equation (4a). Substituting in it the values of  $h$  from equation (9), of  $K$  from equation (3), and of  $C$  from equation (8) yields

$$\begin{aligned} \frac{144W}{2\pi M_p \tan \alpha_e} &= \frac{2r_e \tan^2 \delta}{4 \sin^3 \alpha_e \cos^2 \beta} \\ &+ \frac{\sqrt{2} \tan \delta}{2 \sin^{3/2} \alpha_e \cos \beta} r_e \sqrt{\frac{2 \tan^2 \delta}{\sin^3 \alpha_e \cos^2 \beta} - \frac{4 \tan \varphi}{\cos \beta}} \\ &+ \frac{r_e^2}{4r_e} \left( \frac{2 \tan^2 \delta}{\sin^3 \alpha_e \cos^2 \beta} - \frac{4 \tan \varphi}{\cos \beta} \right) \end{aligned}$$

and, after division by  $r_e$  and rearrangement,

$$\begin{aligned} \frac{144W \cot \alpha_e}{2\pi M_p r_e} &= \frac{\tan^2 \delta}{\sin^3 \alpha_e \cos^2 \beta} - \frac{\tan \varphi}{\cos \beta} \\ &+ \frac{\tan \delta}{\sqrt{2} \sin^3 \alpha_e \cos \beta} \sqrt{\frac{2 \tan^2 \delta}{\sin^2 \alpha_e \cos^2 \beta} - \frac{4 \tan \varphi}{\cos \beta}} \end{aligned} \quad (17)$$

#### REFERENCES

1. Patterson, G. N.: Modern Diffuser Design. Aircraft Engineering, vol. X, no. 115, Sept. 1938, pp. 267-273.
2. Polikovsky, V., and Nevelson, M.: The Performance of a Vaneless Diffuser Fan. NACA TM No. 1038, 1942.
3. Ellerbrock, Herman H., and Goldstein, Arthur W.: Principles and Methods of Rating and Testing Centrifugal Superchargers. NACA ARR, Feb. 1942.

4. NACA Subcommittee on Supercharger Compressors: Standard Method of Graphical Presentation of Centrifugal Compressor Performance. NACA ARR No. E5F13a, 1945.
5. NACA Subcommittee on Supercharger Compressors: Standard Procedures for Rating and Testing Centrifugal Superchargers. NACA ARR No. E5F13, 1945.
6. Schüle, W.: Technical Thermodynamics. Sir Issac Pitman and Sons (London), 1933, p. 301.

TABLE I - PASSAGE HEIGHTS THROUGH DIFFUSERS WITH  
DIFFERENT EQUIVALENT CONE ANGLES

Radius to rear shroud (in.)	Passage height, h (in.)		
	Equivalent cone angle, $\delta$ (deg)		
	4	6	8
5.350	0.806	0.806	0.806
5.519	.782	.782	.782
6.000	.699	.699	.699
6.290	.632	.632	.632
6.700	.574	.579	.584
7.000	.564	.576	.588
7.500	.549	-----	-----
8.000	.536	.571	.605
9.000	.517	.570	.624
10.000	.503	.572	.646
11.000	.492	.577	.668
12.000	.485	.584	.692
13.000	.480	.593	.717
13.500	.478	.598	.729
17.000	.474	.636	.820

National Advisory Committee  
for Aeronautics

TABLE II - RADII THROUGH DIFFUSERS WITH DIFFERENT  
EQUIVALENT CONE ANGLES

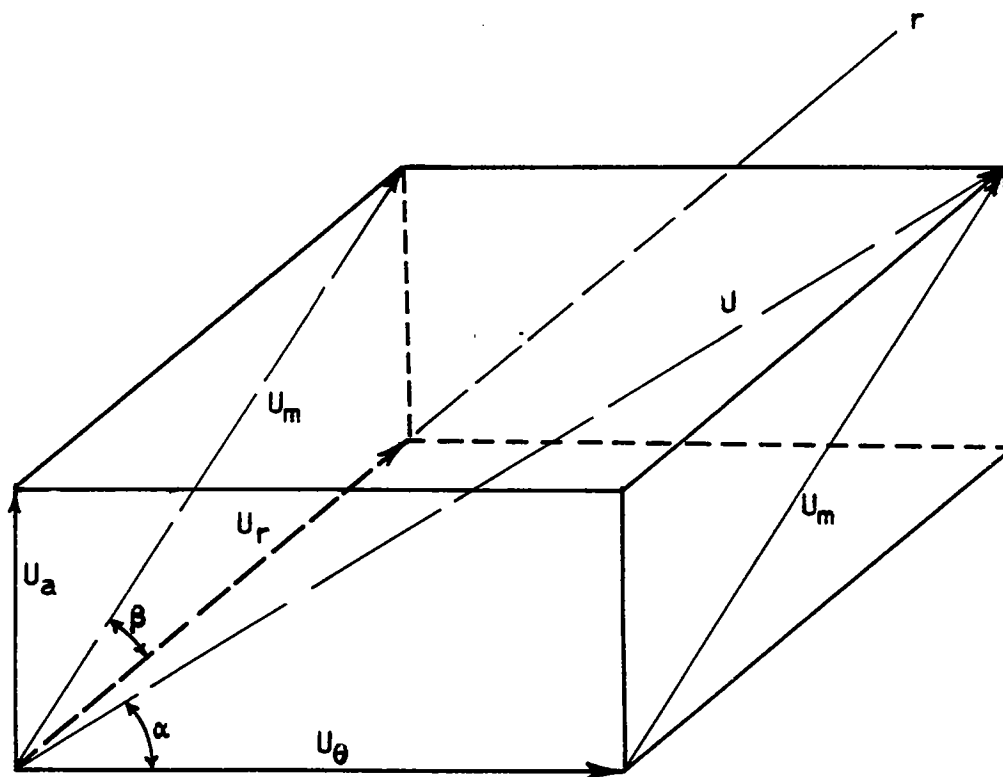
Radius to rear shroud (in.)	Radius to front shroud (in.)	Mean radius (in.)	Radius to front shroud (in.)	Mean radius (in.)	Radius to front shroud (in.)	Mean radius (in.)
	Equivalent cone angle, $\delta$ (deg)					
	4		6		8	
5.350	5.762	5.556	5.762	5.556	5.762	5.556
5.519	5.907	5.713	5.907	5.713	5.907	5.713
6.000	6.313	6.156	6.313	6.156	6.313	6.156
6.290	6.557	6.423	6.557	6.423	6.557	6.423
6.700	6.943	6.822	6.945	6.822	6.947	6.823
7.000	7.238	7.119	7.244	7.122	7.249	7.125
7.500	7.732	7.616	-----	-----	-----	-----
8.000	8.227	8.113	8.241	8.120	8.256	8.128
9.000	9.218	9.109	9.241	9.120	9.264	9.132
10.000	10.212	10.106	10.242	10.121	10.272	10.136
11.000	11.208	11.104	11.244	11.122	11.282	11.141
12.000	12.205	12.102	12.247	12.123	12.292	12.146
13.000	13.203	13.101	13.251	13.125	13.303	13.151
13.500	13.702	13.601	13.753	13.626	13.808	13.654

National Advisory Committee  
for Aeronautics

TABLE III - PASSAGE HEIGHTS AND RADII THROUGH DIFFUSERS  
WITH DIFFERENT THROAT-INLET RATIOS

Radius to rear shroud (in.)	Radius to front shroud (in.)	Passage height h (in.)	Radius to front shroud (in.)	Passage height h (in.)	Radius to front shroud (in.)	Passage height h (in.)
	Contraction ratio, $\lambda$					
	0.62		0.72		0.93	
5.519	5.907	0.782	5.907	0.782	5.762	0.782
6.000	6.223	.522	6.313	.699	6.322	.763
6.290	6.507	.500	6.557	.632	6.608	.753
6.700	6.911	.498	6.945	.579	7.013	.747
7.000	7.210	.497	7.244	.576	7.310	.735
7.500	7.709	.496	-----	-----	7.806	.725
8.000	8.210	.496	8.241	.571	8.303	.717
9.000	9.211	.500	9.211	.570	9.299	.708
10.000	10.213	.506	10.242	.572	10.297	.703
11.000	11.217	.513	11.244	.577	11.297	.702
12.000	12.221	.523	12.247	.584	12.298	.704
13.000	13.225	.533	13.251	.593	13.300	.709
13.500	13.728	.539	13.753	.598	13.800	.712
17.000	-----	-----	-----	.631	-----	-----

National Advisory Committee  
for Aeronautics



$$U^2 = U_{\theta}^2 + U_r^2 + U_a^2$$

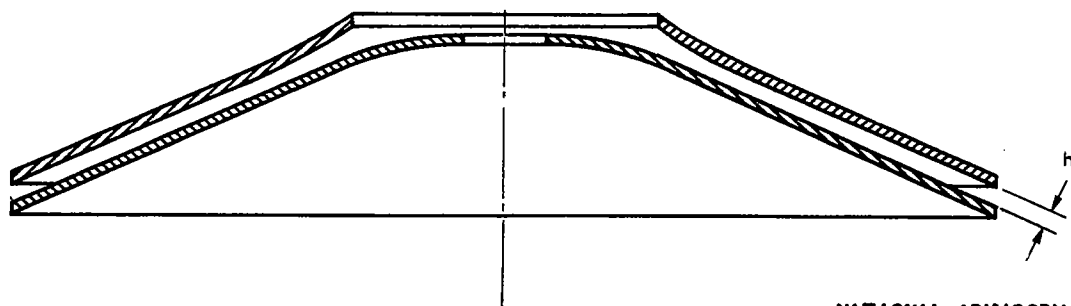
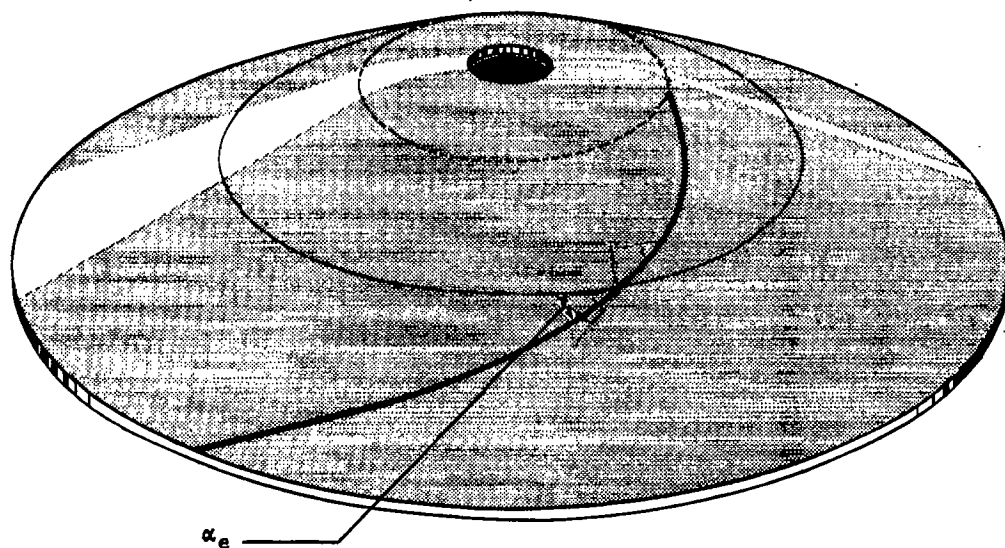
$$\frac{U}{U_m} = \sin \alpha$$

$$\frac{U_{\theta}}{U} = \cos \alpha$$

$$\frac{U}{U_r} = \cos \beta$$

NATIONAL ADVISORY  
COMMITTEE FOR AERONAUTICS

Figure 1. - Velocity relations in vaneless mixed-flow diffuser.

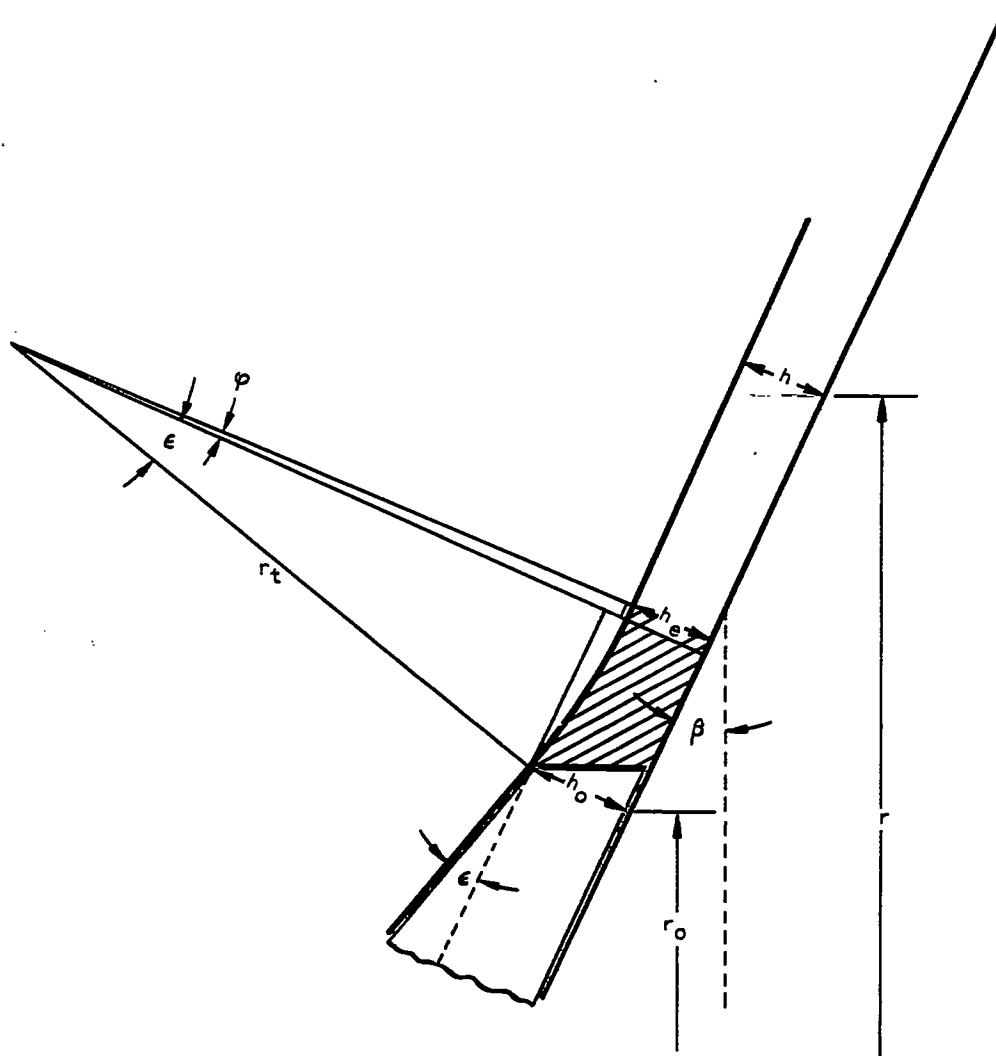


NATIONAL ADVISORY  
COMMITTEE FOR AERONAUTICS

Figure 2. - Vaneless mixed-flow diffuser showing constant angle of logarithmic-spiral flow path and height of diffuser passage.

794  
466

1814826



NATIONAL ADVISORY  
COMMITTEE FOR AERONAUTICS

Figure 3. - Layout of diffuser entrance and transition section.

Fig. 4

NACA TN No. 1426

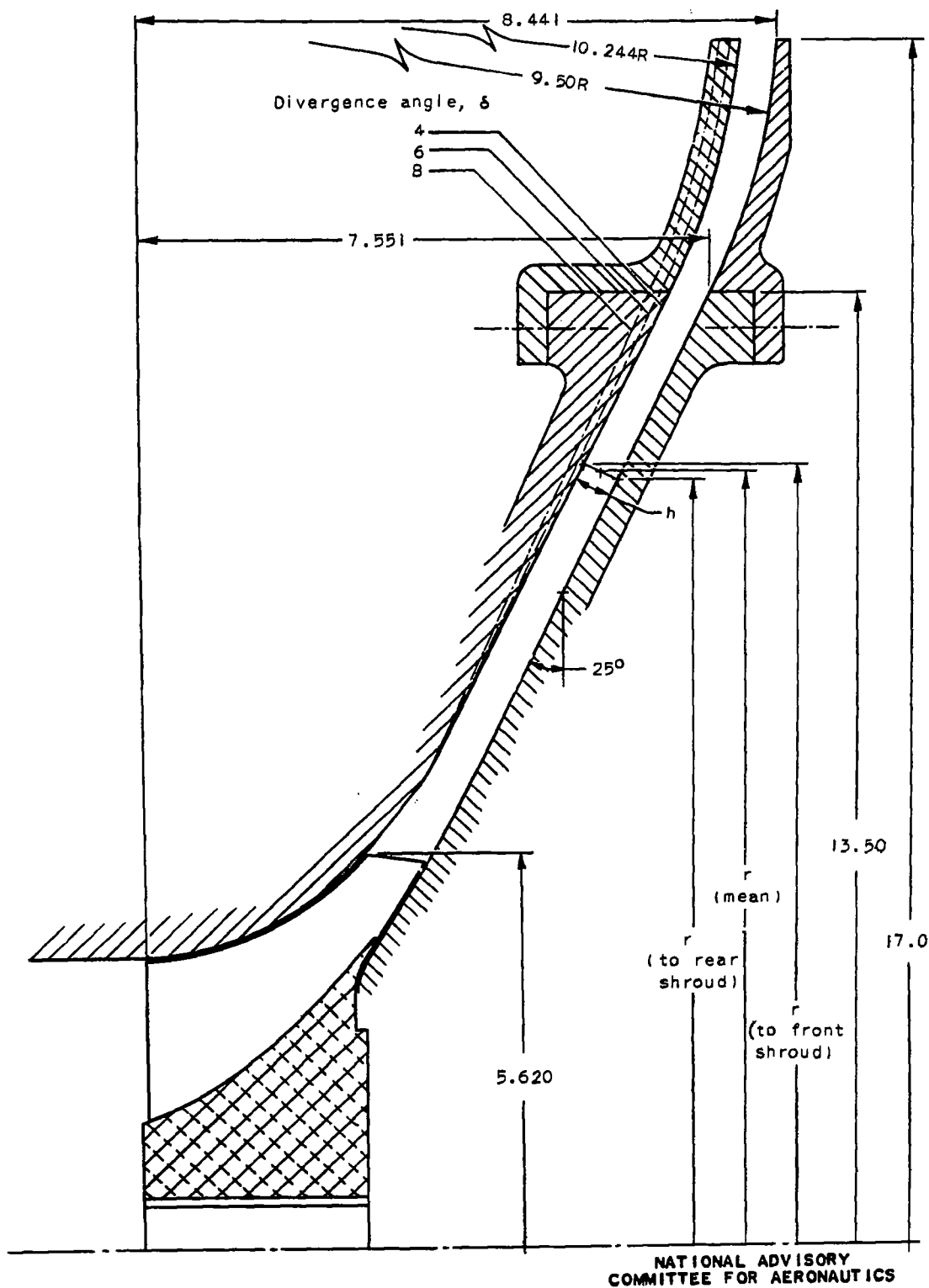
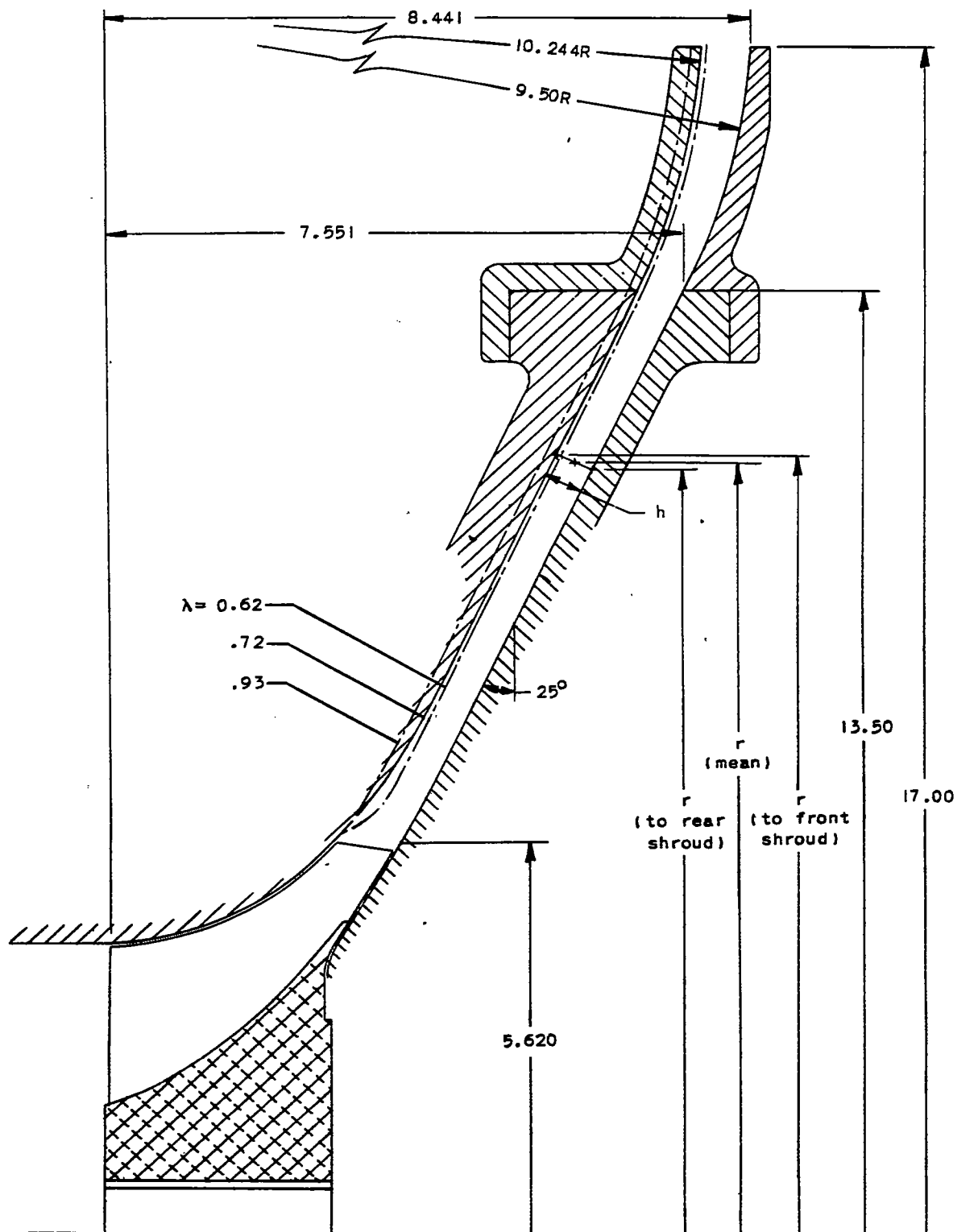


Figure 4. - Section through diffuser passage showing variations in divergence angle. (Dimensions in in. See table I.)

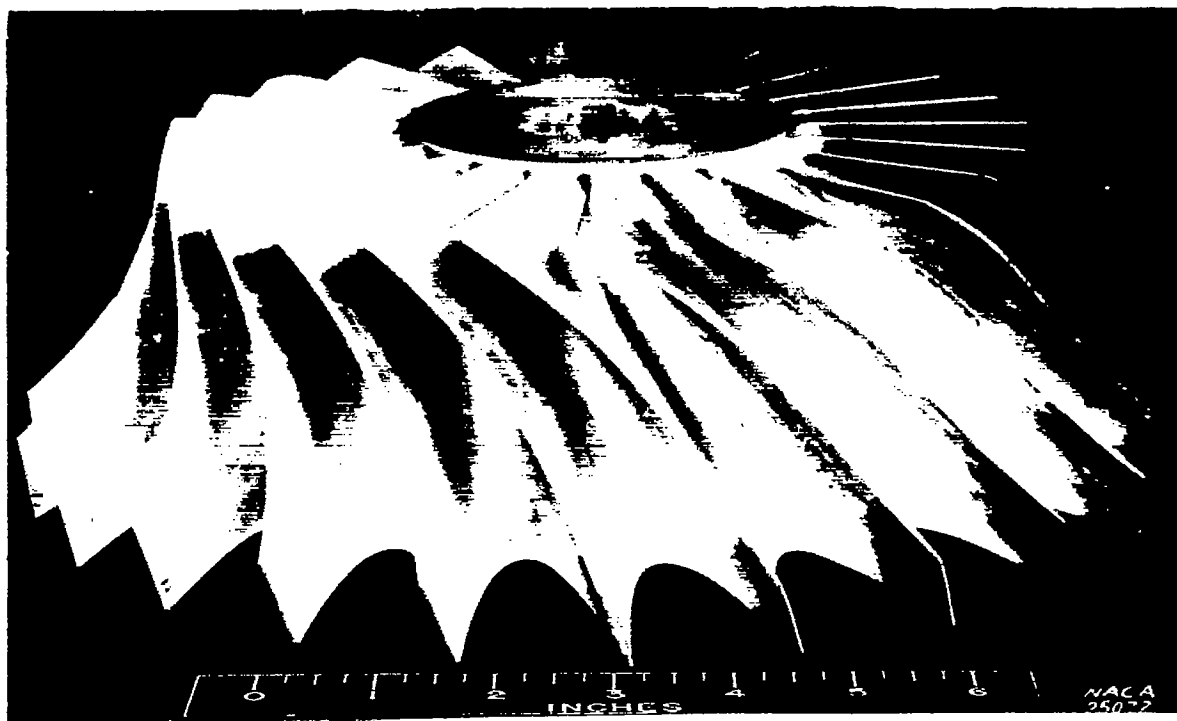
h66

598 + 181

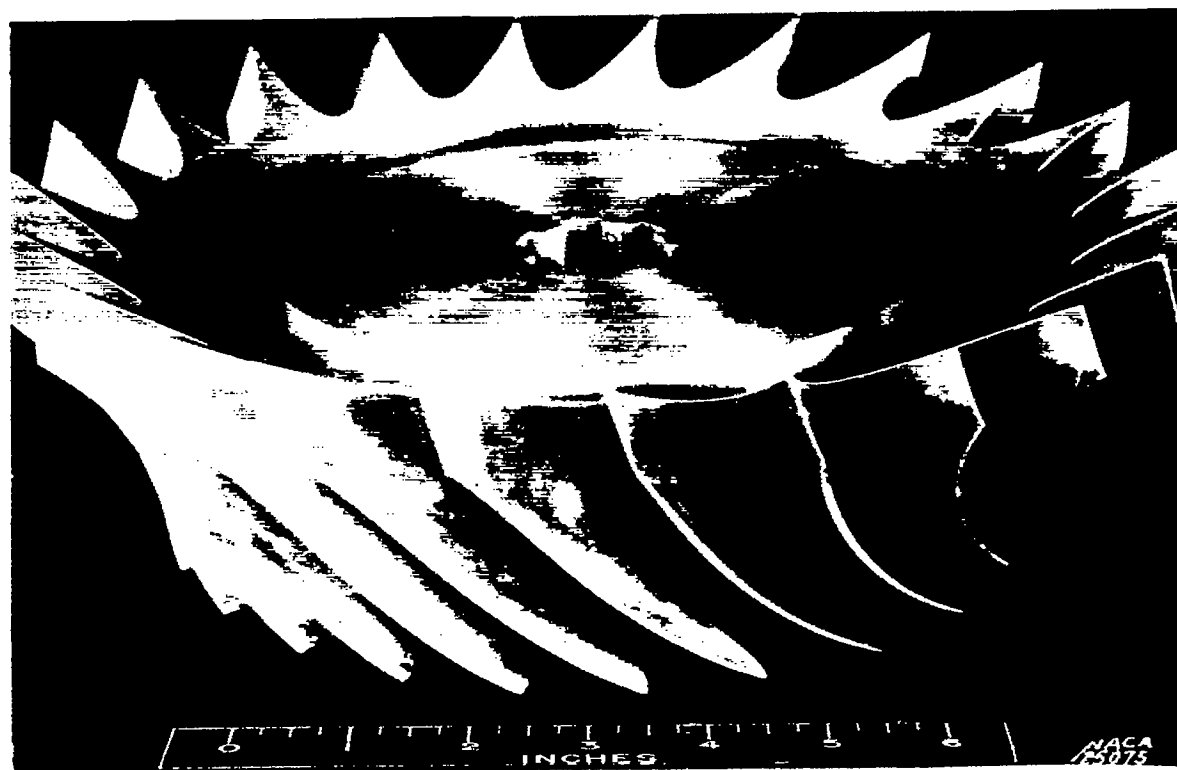


NATIONAL ADVISORY  
COMMITTEE FOR AERONAUTICS

Figure 5. - Section through diffuser passage showing variations in throat size. (Dimensions in in. See tables II and III.)

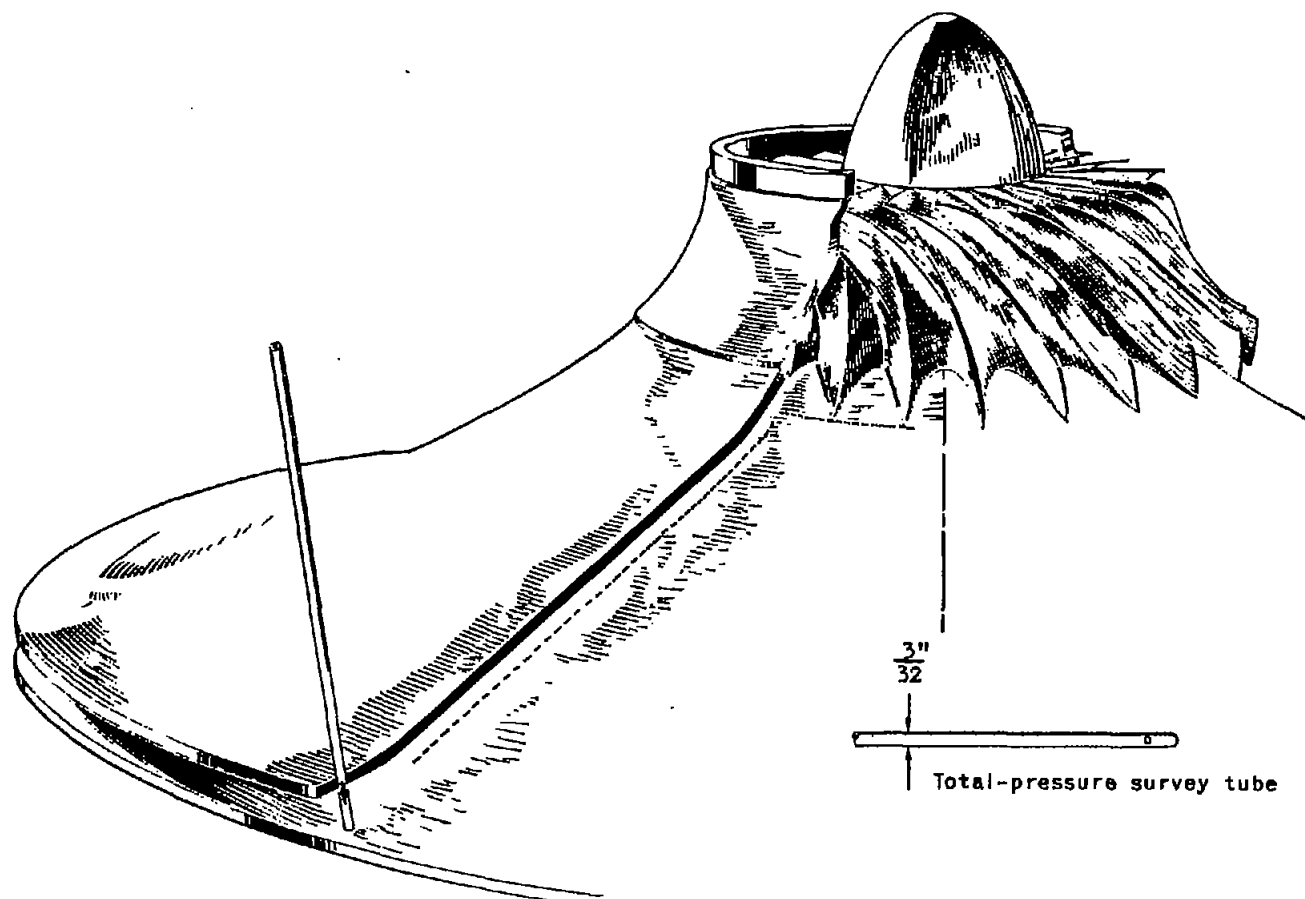


(a) Top view.



(b) Bottom view.

Figure 6. - Mixed-flow impeller used in diffuser investigation.



NATIONAL ADVISORY  
COMMITTEE FOR AERONAUTICS

Figure 7. - Assembly of mixed-flow impeller and vaneless diffuser.

Fig. 8

NACA TN No. 1426

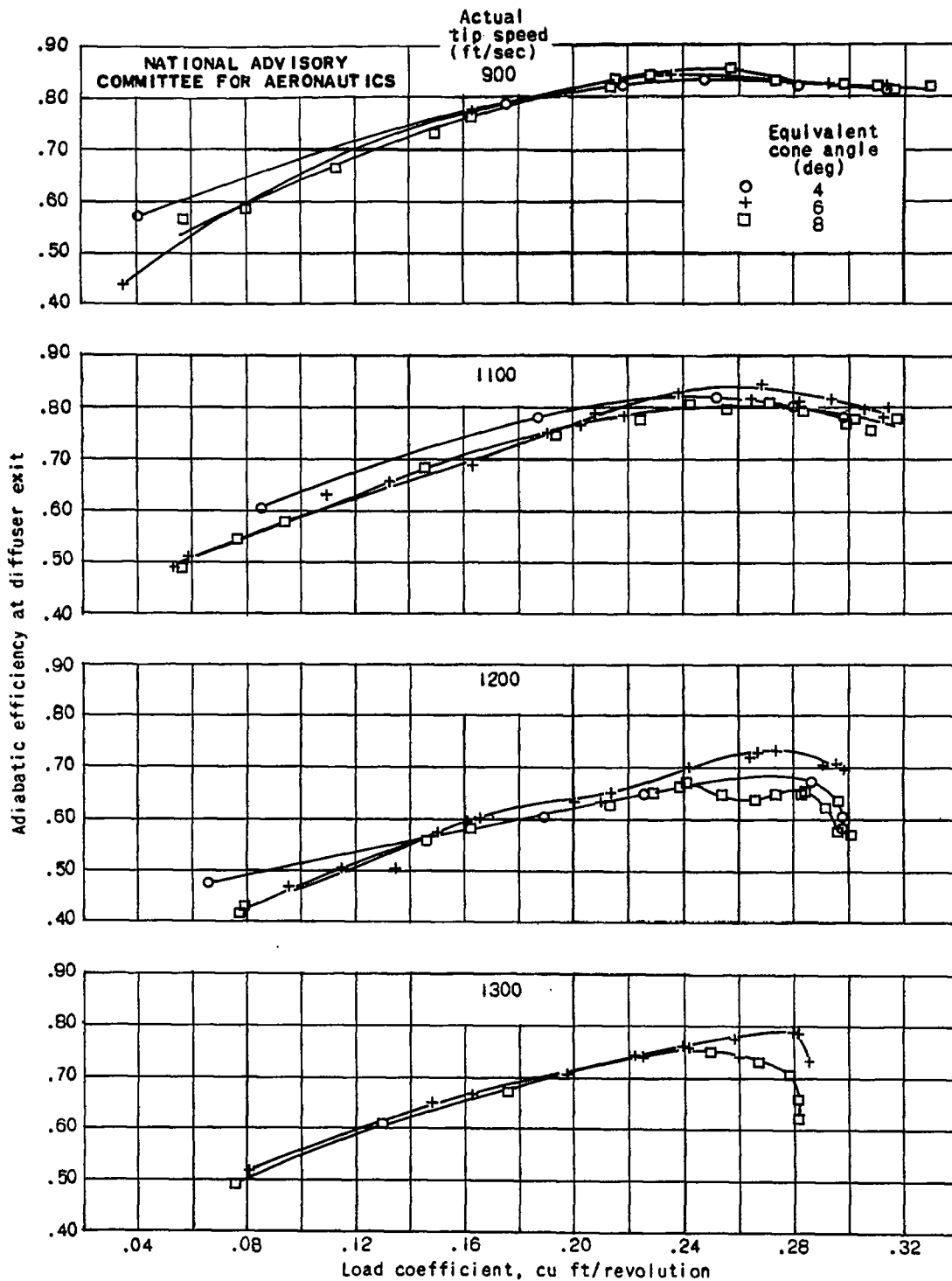


Figure 8. - Adiabatic efficiency at diffuser exit of vaneless mixed-flow diffuser with contraction ratio of 0.72 and three different equivalent cone angles.

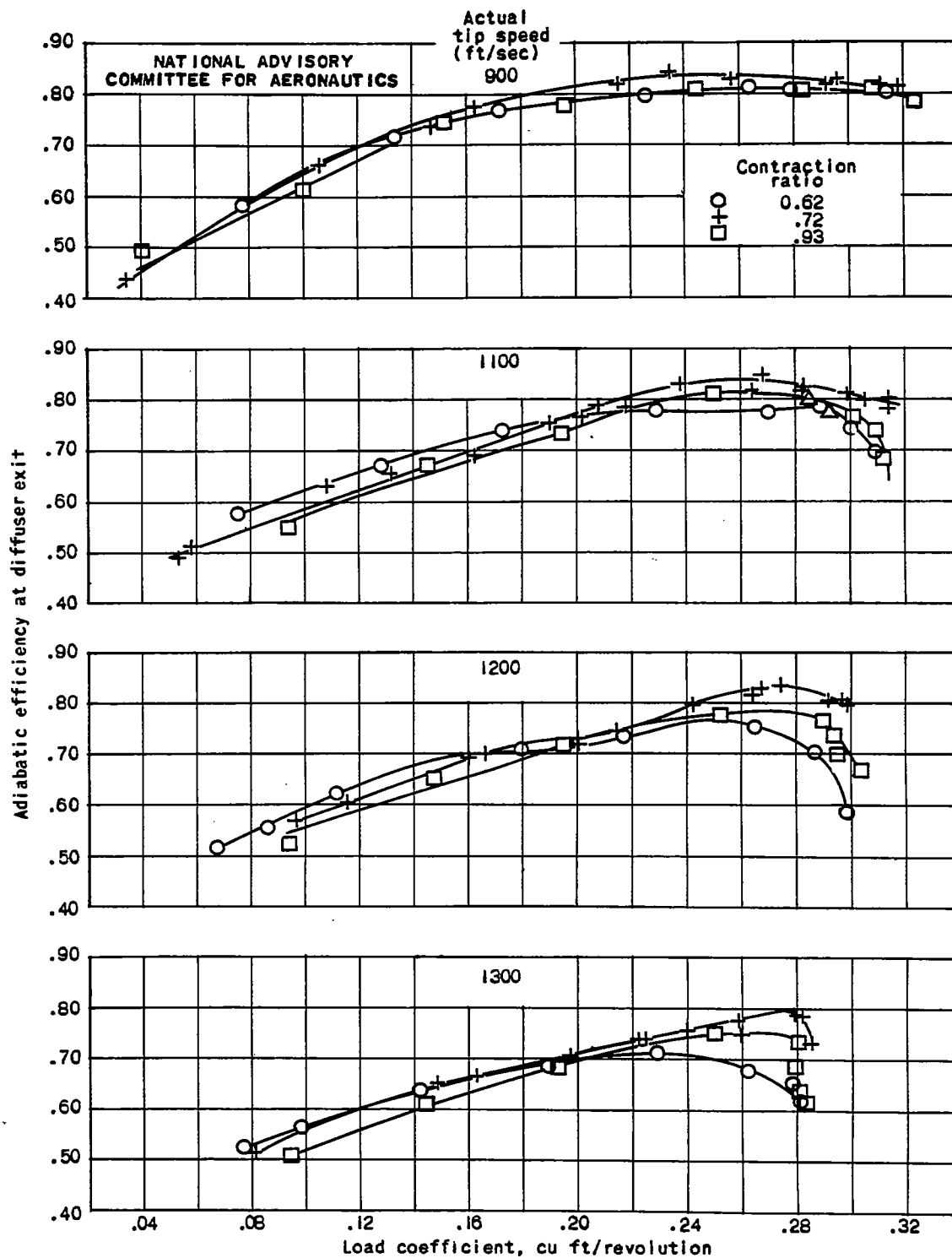


Figure 9. - Adiabatic efficiency at diffuser exit of vaneless mixed-flow diffuser with equivalent cone angle of  $60^\circ$  and three different values of contraction ratio.

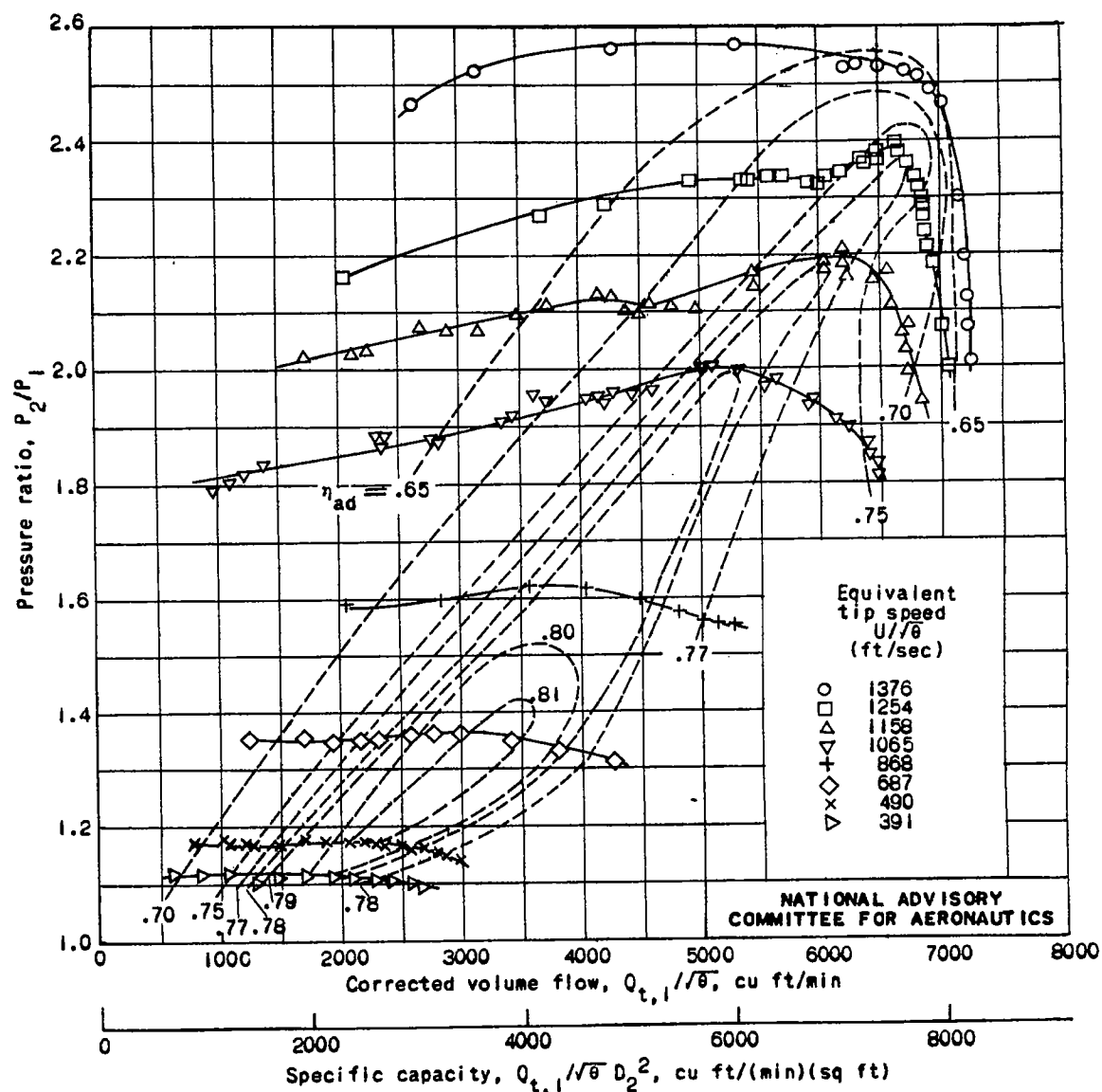


Figure 10. - Performance of compressor with vaneless mixed-flow diffuser with equivalent cone angle of  $6^\circ$  and contraction ratio of 0.72.

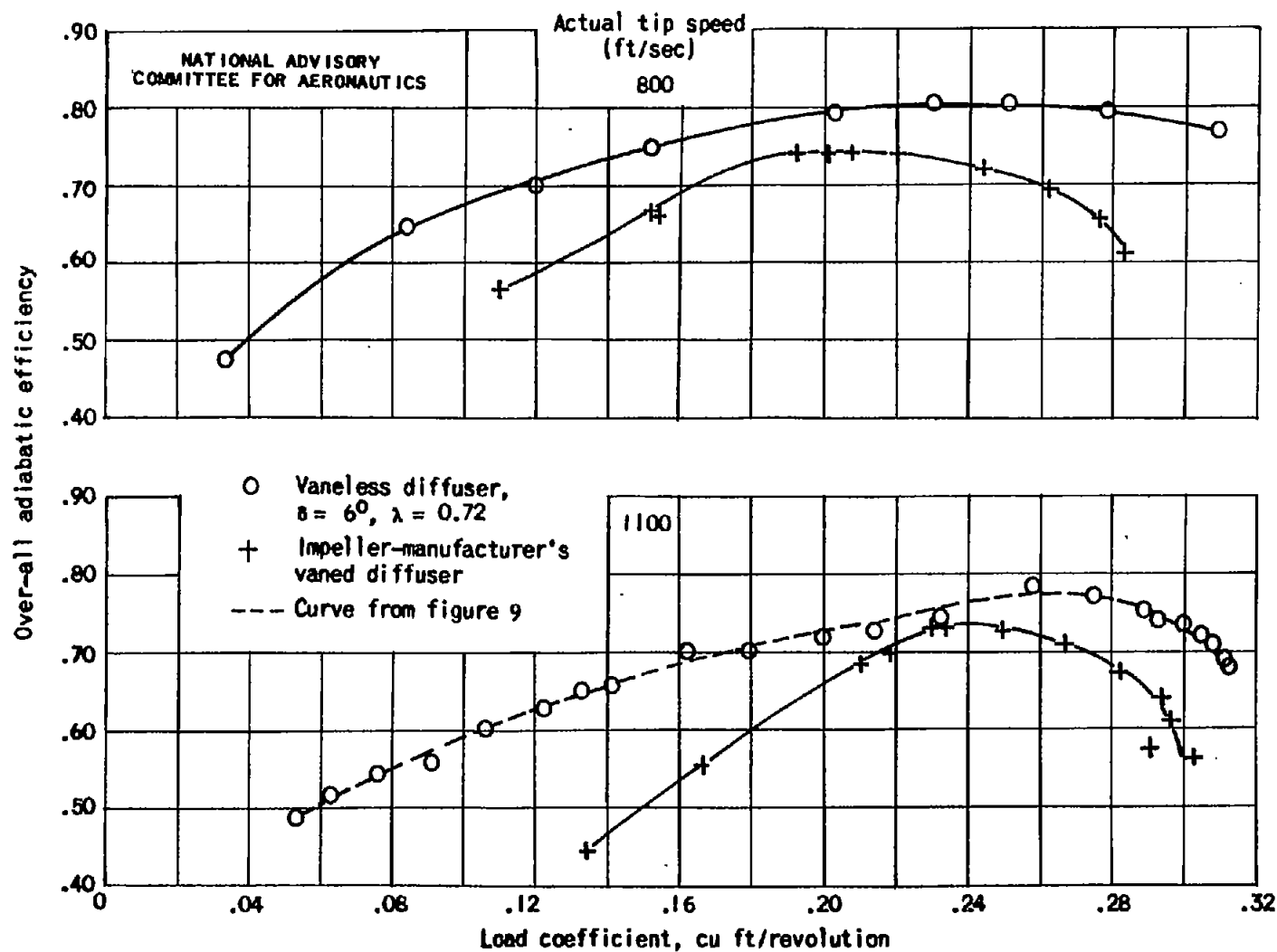


Figure 11. - Performance curves for compressor with vaneless mixed-flow diffuser and with Impeller-manufacturer's vaned diffuser.